Evidence for M_B and M_C phases in the morphotropic phase boundary region of $(1-x)[Pb(Mg_{1/3}Nb_{2/3})O_3]-xPbTiO_3$: A Rietveld study

Akhilesh Kumar Singh and Dhananjai Pandey*
School of Materials Science & Technology, Banaras Hindu University, Varanasi 221 005, India
(Received 10 June 2002; revised manuscript received 14 November 2002; published 6 February 2003)

We present here the results of the room-temperature dielectric measurements and Rietveld analysis of the powder x-ray diffraction data on $(1-x)[Pb(Mg_{1/3}Nb_{2/3})O_3]-xPbTiO_3$(PMN-$x$PT) in the composition range $0.20 \leqslant x \leqslant 0.45$ to show that the morphotropic phase boundary region contains two monoclinic phases with space groups Cm (or M_B type) and Pm (or M_C type) stable in the composition ranges $0.27 \leqslant x \leqslant 0.30$ and $0.31 \leqslant x \leqslant 0.34$, respectively. The structure of PMN-xPT in the composition ranges $0 \leqslant x \leqslant 0.26$ and $0.35 \leqslant x \leqslant 1$ is found to be rhombohedral (R3m) and tetragonal (P4mm), respectively. These results are compared with the predictions of Vanderbilt & Cohen's theory.

DOI: 10.1103/PhysRevB.67.064102 PACS number(s): 77.84.Dy

I. INTRODUCTION

Relaxor ferroelectric based morphotropic phase boundary (MPB) ceramics such as $(1-x)[Pb(Mg_{1/3}Nb_{2/3})O_3]-xPbTiO_3$(PMN$-x$PT) (Ref. 1) and $(1-x)\times[Pb(Zn_{1/3}Nb_{2/3})O_3]-xPbTiO_3$(PZN$-x$PT) (Ref. 2) show much higher electromechanical response about their MPB's in comparison to the well-known $Pb(Zr_xTi_{1-x})O_3$ (PZT) system.[3] The reason why relaxor based MPB systems have much higher electromechanical response is still not very clear eventhough recent theoretical and experimental developments in PZT have improved our understanding of the phase stabilities in the vicinity of the MPB.[4–12] Noheda *et al.* have discovered that the tetragonal phase of PZT with compositions ($x=0.50,\ 0.52$) close to the MPB transforms to a monoclinic phase with space group Cm at low temperatures.[4,5] Ragini *et al.*[6] and Ranjan *et al.*[7] have discovered yet another low-temperature phase transition, in which the Cm monoclinic phase transforms to another monoclinic phase with Cc space group.[8] The Cm to Cc phase transition is an antiferrodistortive (AFD) transition leading to superlattice reflections which are observable in the electron[6] and neutron[7] diffraction patterns only, and not in the x-ray diffraction (XRD) patterns as a result of which Noheda *et al.* missed the Cc phase in their high resolution XRD studies at low temperatures. The tetragonal to Cm, and Cm to Cc transitions are accompanied with pronounced anomalies in the elastic constant and dielectric constant.[6] It has been argued[9–11] that the monoclinic Cm phase provides the path for polarization rotation between tetragonal (P4mm) and rhombohedral (R3m) phases. X-ray Rietveld analysis by Ragini *et al.*,[12] has, however, revealed that the hitherto believed rhombohedral phase of PZT for $0.53<x<0.62$ (Ref. 13,14) is indeed monoclinic (Cm) with very small domain size leading to composition-dependent anomalous broadening of various reflections. Thus the MPB in the PZT system separates the stability fields of tetragonal and monoclinic Cm phases.[12] On application of dc field, these monoclinic domains get aligned and merged as a result of which some of the XRD peaks showing anomalous broadening in the unpoled state start exhibiting splittings characteristic of the Cm phase in the poled state. Thus, according to Ragini *et al.*,[12,15] the field-induced rhombohedral to Cm transition reported by Guo *et al.*[11] is really a transition from a small-domain Cm phase to large-domain Cm phase. Based on Rietveld analysis of the XRD data, Ragini *et al.*[12] have also shown that the tetragonal and monoclinic (Cm) phases coexist across the MPB in the composition range $0.520 \leqslant x \leqslant 0.525$ due to nucleation barrier to the first-order transition between the high-temperature tetragonal and the low-temperature monoclinic Cm phases.[15]

These recent developments in PZT have been followed up by similar studies on the structure of MPB phases in the PMN-xPT (Refs. 16–20) and PZN-xPT (Refs. 21,22) systems. In these systems also, the structure of the morphotropic phase in the unpoled state is monoclinic but with a space group Pm,[16,17] which is different from that in the PZT system. The Pm space group proposed by Singh and Pandey[16] and Kiat *et al.*[17] in the MPB region of the PMN-xPT system has recently been confirmed in the high resolution powder XRD studies by Noheda *et al.*[23] contradicting an earlier report of Cm space group by the same workers for a similar composition.[19] However, in the PZN-xPT system, the possibility of monoclinic Pm[17] or orthorhombic Bmm2[21] structures in the MPB region continues to be debated. More interestingly, Noheda *et al.*[24] and Ohwada *et al.*[25] have observed a field-induced irreversible rhombohedral to Pm monoclinic phase transition in PZN-0.08PT through the Cm monoclinic phase.

Using eighth-order expansion of the Devonshire theory, Vanderbilt and Cohen[26] have predicted different regions of stability for the monoclinic Pm and Cm phases that are designated as M_C and M_A/M_B, respectively, in their paper. Although both M_A and M_B phases belong to the Cm space group, the difference lies in the magnitudes of the components of the polarization (P) corresponding to the pseudocubic cell. For the M_A phase $P_X=P_Y\neq P_Z$ with $P_Z>P_X$, while for the M_B phase, $P_X=P_Y\neq P_Z$ with $P_Z<Px$. As per the phase diagram of Vanderbilt and Cohen,[26] one expects a narrow stability field of the M_B phase between the rhombohedral and M_C phases. The present work was undertaken to verify the existence of the Cm (M_B) phase for compositions

in between those for the rhombohedral and monoclinic (Pm) phases using the Rietveld analysis of x-ray powder diffraction data on PMN-xPT samples with x varying from 0.26 to 0.39 at an interval of $\Delta x = 0.01$. From a careful study of the variation of the dielectric constant and crystal structure with composition (x) on unpoled PMN-xPT ceramics, we show that the dominant phases in the composition ranges $0 \leqslant x \leqslant 0.26$, $0.27 \leqslant x \leqslant 0.30$, $0.31 \leqslant x \leqslant 0.34$, and $0.35 \leqslant x \leqslant 1$ are rhombohedral (R3m), monoclinic M_B (Cm), monoclinic M_C (Pm) and tetragonal (P4mm), respectively, in reasonable agreement with the predictions of Vanderbilt and Cohen's theory.[26]

II. EXPERIMENT

Samples used in the present work were prepared by a modified solid state route.[27] One of the common problems associated with the solid-state synthesis of PMN-xPT ceramics is the appearance of an unwanted pyrochlore phase.[28] To get rid of this unwanted phase, off-stoichiometric compositions, with excess of MgO and PbO, are used.[29] For example, Noheda *et al.*[23] have used 15.5 and 2 wt% excess of MgO and PbO for getting pure perovskite phase. This naturally perturbs the phase stabilities in the vicinity of the MPB where the crystal structure is very sensitive to even small variations in the composition because of nearly degenerate nature of various phases. In order to bring out the intrinsic features of the PMN-xPT system, it is imperative to prepare pyrochlore phase free PMN-xPT ceramics in stoichiometric compositions (i.e., without using any excess of PbO and MgO). We have achieved this by using $PbCO_3$ and $MgCO_3 \cdot 3H_2O$, instead of PbO and MgO, respectively, and introducing one more step in the reaction sequence for mixing of TiO_2.[27] In the present work, AR grade Nb_2O_5 (99.95%), TiO_2 (99%), $Mg(NO_3)_2 \cdot 6H_2O$ (99%), $Pb(NO_3)_2$ (99%), and ammonium carbonate were used. $MgCO_3 \cdot 3H_2O$ and $PbCO_3$ were prepared from $Mg(NO_3)_2 \cdot 6H_2O$ and $Pb(NO_3)_2$ by precipitation. Mixing of various ingredients in stoichiometric proportions was carried out for 6 h using a ball mill (Retsch, Japan) with zirconia jars and zirconia balls. AR grade acetone was used as the mixing media. Heat treatments for calcination were carried out in alumina crucibles using a globar furnace. The columbite precursor $MgNb_2O_6$ (MN) (Ref. 28) was prepared by calcining a stoichiometric mixture of $MgCO_3 \cdot 3H_2O$ and Nb_2O_5 at 1050°C for 6 h. At the next stage, stoichiometric amount of TiO_2 was mixed with $MgNb_2O_6$ and the mixture was calcinated at 1050°C for 6 h to obtain $[(1-x)/3]MgNb_2O_6 - (x)TiO_2$ (MNT) precursor. This MNT precursor was then mixed with stoichiometric amount of $PbCO_3$ and calcined at 750°C for 6 h. The powder obtained at this stage consists of pure perovskite phase of PMN-xPT free from the pyrochlore phase. Cold compaction of calcined powders was done using a steel die of 12-mm diameter and an uniaxial hydraulic press at an optimized load of 65 kN. 2% polyvinyl alcohol solution in water was used as binder. The green pellets were kept at 500°C for 10 h to burn off the binder material and then sintered at 1150°C for 6 h in sealed crucibles with controlled PbO atmosphere. Density of the sintered pellets was higher than 98% of the theoretical density. Sintered pellets were crushed into fine powders and then annealed at 500°C for 10 h to remove the strains introduced during crushing for x-ray characterizations. XRD measurements were carried out using a 12 kW rotating anode (Cu) based Rigaku powder diffractometer operating in the Bragg-Brentano geometry and fitted with a graphite monochromator in the diffracted beam. Fired-on silver paste was used for electroding the sintered pellets. The dielectric measurements at 1 kHz were carried out using a HIOKI 3532 LCR HiTester.

III. DETAILS OF THE RIETVELD REFINEMENT

Rietveld refinement was carried out using DBWS-9411 program[30] except for the section 5.7, where GSAS program package[31] was used which incorporates anisotropic peak shape proposed by Stephens.[32] In all other refinements pseudo-Voigt function was used to define the peak profiles while a fifth-order polynomial was used for describing the background. Except for the occupancy parameters of the ions, which were kept fixed at the nominal composition, all other parameters i.e., scale factor, zero correction, background, half-width parameters along with mixing parameters, lattice parameters, positional coordinates, and isotropic thermal parameters were refined. The isotropic thermal parameter values for Pb was invariably found to be high as reported by Kiat *et al.* also.[17] Use of anisotropic thermal parameters for Pb did not lead to any improvement in the agreement factors.

In the tetragonal phase with P4mm space group, the Pb^{2+} ion occupies $1(a)$ sites at $(0,0,z)$, $Ti^{4+}/Nb^{5+}/Mg^{2+}$ and O_I^{2-} occupy $1(b)$ sites at $(1/2,1/2,z)$, and O_{II}^{2-} occupy 2(c) sites at $(1/2,0,z)$. For the rhombohedral phase with R3mH space group, we used hexagonal axes with lattice parameters $a_H = b_H = \sqrt{2}a_R$ and $c_H = \sqrt{3}a_R$, where a_R corresponds to the rhombohedral cell parameter. In the asymmetric unit of the structure of the rhombohedral phase with R3mH space group, Pb^{2+} and $Nb^{5+}/Ti^{4+}/Mg^{2+}$ ions occupy $3(a)$ sites at $(0,0,z)$ and O^{2-} at the $9(b)$ site at $(x,2x,z)$. In the monoclinic phase with space group Cm, there are four ions in the asymmetric unit with Pb^{2+},$Ti^{4+}/Nb^{5+}/Mg^{2+}$ and O_I^{2-} in $2(a)$ sites at $(x,0,z)$ and O_{II}^{2-} in $4(b)$ sites at (x,y,z). The asymmetric unit of the monoclinic phase with space group Pm has got five ions with Pb^{2+} and O_I^{2-} in 1(a) site at $(x,0,z)$, $Ti^{4+}/Nb^{5+}/Mg^{2+}$,O_{II}^{2-} and O_{III}^{2-} in $1(b)$ sites at $(x,1/2,z)$. Following the established conventions, Pb^{2+} was fixed at (0,0,0) for the tetragonal[33] and monoclinic[4,16] structures. Following Megaw and Darlington,[34] the z coordinate of O^{2-} was fixed at 1/6 for the rhombohedral structure. Additionally, space group Bmm2 was also taken into consideration for a few compositions. For this space group, Pb^{2+} ion occupies $2(b)$ sites at $(1/2,1/2,z)$,$Nb^{5+}/Ti^{4+}/Mg^{2+}$ ions occupy $2(a)$ sites at $(0,0,z)$,O_I^{2-} in $4(d)$ sites at $(x,0,z)$ and O_{II}^{2-} in the $2(b)$ sites at $(0,1/2,z)$. $Nb^{5+}/Ti^{4+}/Mg^{2+}$ ions were kept at the origin (0,0,0) for the refinement.[35]

IV. LOCATION OF THE MORPHOTROPIC PHASE BOUNDARY

Lead magnesium niobate (PMN) is a relaxor ferroelectric with very high value of room temperature dielectric constant

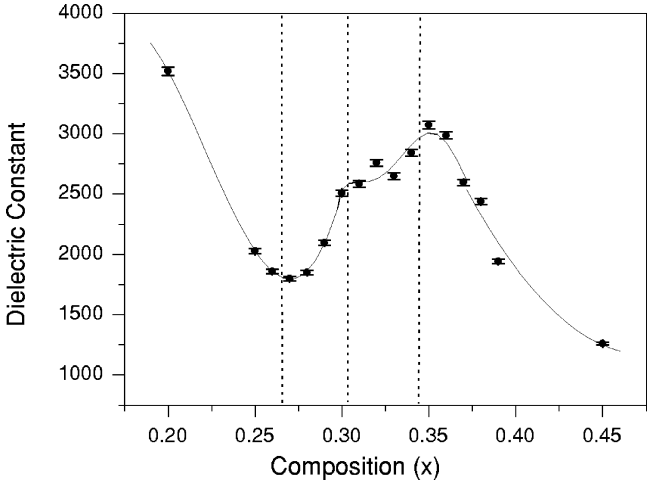

FIG. 1. Variation of the real part of the dielectric constant (ϵ') with composition (x) at room temperature for PMN-xPT ceramics.

($\approx$12 000 in ceramic form).[36] With the addition of lead titanate (PT), whose dielectric constant is very low (<400),[3] it is expected that the dielectric constant of the resulting solid solution will decrease in comparison with PMN with increasing PT content. Figure 1 shows the variation of room-temperature dielectric constant ϵ' with composition (x) for the PMN-xPT ceramics in the composition range $0.20 \leqslant x \leqslant 0.45$. As expected, dielectric constant decreases with increasing value of x up to $x=0.26$. However, from $x=0.27$, the ϵ'-x plot takes an upward trend marking the onset of the MPB region. This upward trend continues upto $x \approx 0.30$, and thereafter shows a plateau region for $0.30<x<0.34$. Kelly *et al.*[37] have also observed a similar plateau region but in poled PMN-xPT samples. The dielectric constant again shows an upward trend leading to a peak around $x=0.35$, and thereafter it decreases monotonically with increasing x. The results shown in this figure correspond to averaging over at least five samples for each composition. The sample to sample variation of dielectric constant for each composition was less than 1% for various PMN-xPT samples. In analogy with the well-known PZT system,[3] the observation of peak in dielectric response at room tempereature as a function of composition confirms the MPB characteristic of the PMN-xPT. However, unlike PZT where one observes only one peak, we have found evidence for two peaks in the PMN-xPT system.

Figure 1 reveals the presence of four different regions. For correlating these regions with a corresponding change in the crystal structure as a function of composition (x), we present in Fig. 2 the powder XRD profiles of the 200, 220, and 222 pseudocubic reflections for various PMN-xPT compositions. In all these profiles, the $K\alpha 2$ component has been removed by using a standard software. For the composition range $0.20 \leqslant x \leqslant 0.26$, the 200 is a singlet, while 220 and 222 are doublets with weaker reflections occurring on the lower 2θ side. This characterizes a rhombohedral phase that is stable for $x \leqslant 0.26$. For $x>0.26$, the width of the 200 profile increases eventually leading to an asymmetric tail on the higher 2θ side which has become quite apparent for $x=0.29$ and 0.30. As shown in the following section, Rietveld

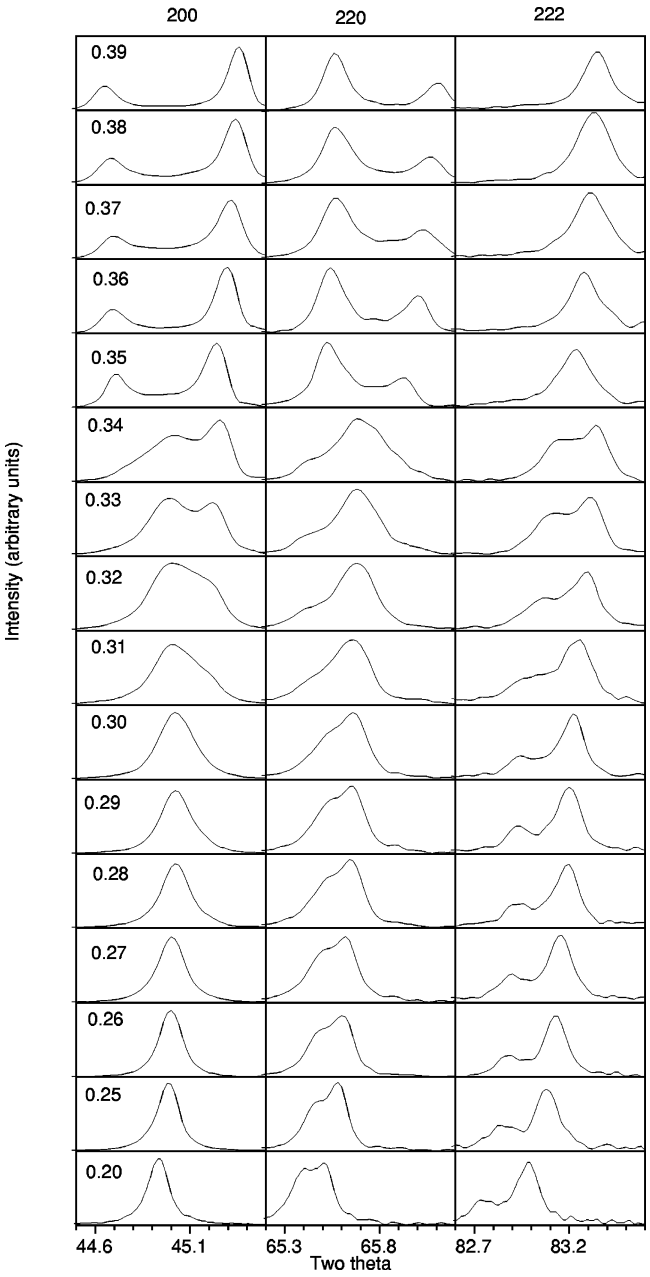

FIG. 2. Evolution of the x-ray diffraction profiles of the 200, 220, and 222 pseudocubic reflections (corresponding to CuKα1 only) with composition (x) for PMN-xPT ceramics.

analysis of the XRD data reveals that the structure of the dominant phase in the composition range $0.26<x<0.31$ is monoclinic (M_B type) with Cm space group. The nature of the 200 profile again changes around $x=0.31$ leading to the appearance of a shoulder on the higher 2θ side which eventually becomes a distinct peak with increasing x as can be seen from Fig. 2 for $0.30<x<0.35$. In this composition range, the dominant phase is monoclinic (M_C type) with Pm space group.[16] For $x \geqslant 0.35$, the profiles shown in Fig. 2 exhibit further changes. In particular, 200 pseudocubic reflection splits into 002 and 200/020 with nearly 1:2 intensity ratio. Further, the shoulder/peak on the lower 2θ side of the 220 pseudocubic profile is replaced by a distinct peak on the

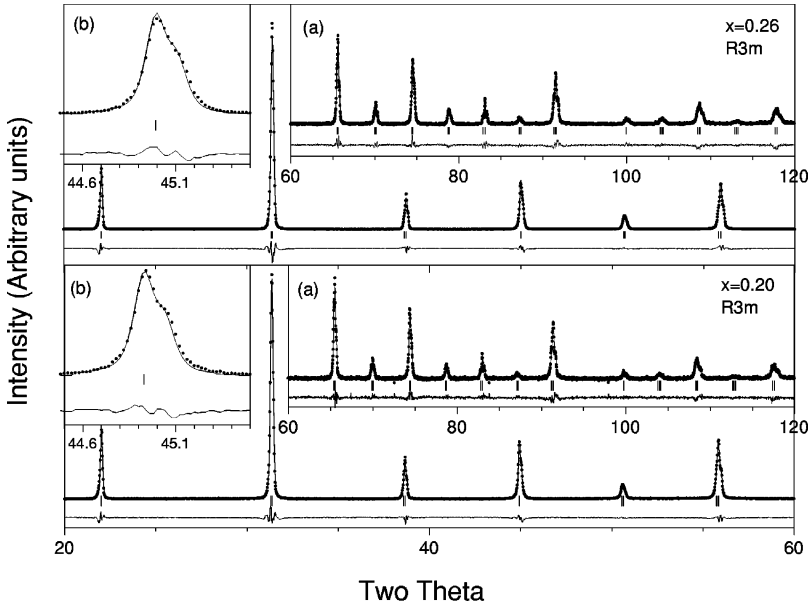

FIG. 3. Observed (dots), calculated (continuous line), and difference (bottom line) profiles obtained after the Rietveld refinement of PMN-xPT with $x=0.20$ and $x=0.26$ using rhombohedral space group R3m in the 2θ range 20–60 deg. Inset (a) shows the patterns in the 2θ range of 60–120 deg while inset (b) illustrates the quality of fit for the 200 reflection. Tick marks above the difference profle show peak positions for CuKα1.

higher 2θ side. In addition, the 222 profile becomes a singlet. All these features correspond to the tetragonal structure, and hence the dominant phase for $x \geqslant 0.35$ is tetragonal, as confirmed by the Rietveld analysis also, the results of which are presented in the following section. Thus the different regions shown in Fig. 1 correspond to four different crystallographic phases of PMN-xPT, which are stable over different ranges of composition.

V. RIETVELD ANALYSIS OF XRD DATA

A. Rhombohedral structure with space group $R3mH$ ($0 \leqslant x \leqslant 0.26$)

Figure 3 depicts the observed, calculated and difference profiles obtained by Rietveld analysis of the XRD data for PMN-xPT with $x=0.20$ and 0.26 using rhombohedral space group R3mH. The fit between the observed and calculated profiles is quite good confirming the rhombohedral structure of PMN-xPT for $x \leqslant 0.26$ in region I of Fig. 1. The refined structural parameters and various agreement factors are given in Table I.

B. Monoclinic structure with space group Cm ($0.27 \leqslant x \leqslant 0.30$)

For compositions with $x \geqslant 0.27$, the 200 reflection becomes broader which cannot be accounted for in terms of the rhombohedral structure for which 200 is a singlet. This anomalous broadening is similar to that reported in $Pb(Fe_{0.5}Nb_{0.5})O_3$ (Ref. 38) and PZT with $0.530 \leqslant x \leqslant 0.60$,[12] where it has been attributed to the Cm phase. The anomalous broadening is absent for $x \leqslant 0.26$ as can be seen from the excellent fit shown in the insets of Fig. 3(b) for the 200 profile. To determine the true symmetry in the composition range $0.27 \leqslant x \leqslant 0.30$, we first carried out Rietveld refinements using various plausible space groups i.e., rhombohedral R3mH, monoclinic Cm, monoclinic Pm, and orthorhombic Bmm2. Figure 4 shows the observed, calculated, and

TABLE I. Refined structural parameters of PMN-xPT for $x=0.20$ and 0.26 using rhombohedral space group R3mH.

Composition (x)	Ions	Positional coordinates			Thermal parameters
		X	Y	Z	B(Å^2)
0.20	Pb^{2+}	0.00	0.00	0.542(1)	3.02(1)
0.26	Pb^{2+}	0.00	0.00	0.546(1)	2.91(2)
0.20	$Ti^{4+}/Nb^{5+}/Mg^{2+}$	0.00	0.00	0.02(2)	0.61(7)
0.26	$Ti^{4+}/Nb^{5+}/Mg^{2+}$	0.00	0.00	0.019(1)	0.14(4)
0.20	O^{2-}	0.353(3)	0.176(3)	0.1667	0.0(1)
0.26	O^{2-}	0.325(3)	0.162(3)	0.1667	0.3(1)
0.20	$a=b=5.6921(1)$(Å)			$c=6.9882(2)$(Å)	
0.26	$a=b=5.6841(1)$(Å)			$c=6.9800(1)$(Å)	
0.20	$R_{WP}=14.76$	$R_{exp}=6.46$		$R_B=10.12$	$\chi^2=5.06$
0.26	$R_{WP}=12.98$	$R_{exp}=7.45$		$R_B=9.93$	$\chi^2=3.01$

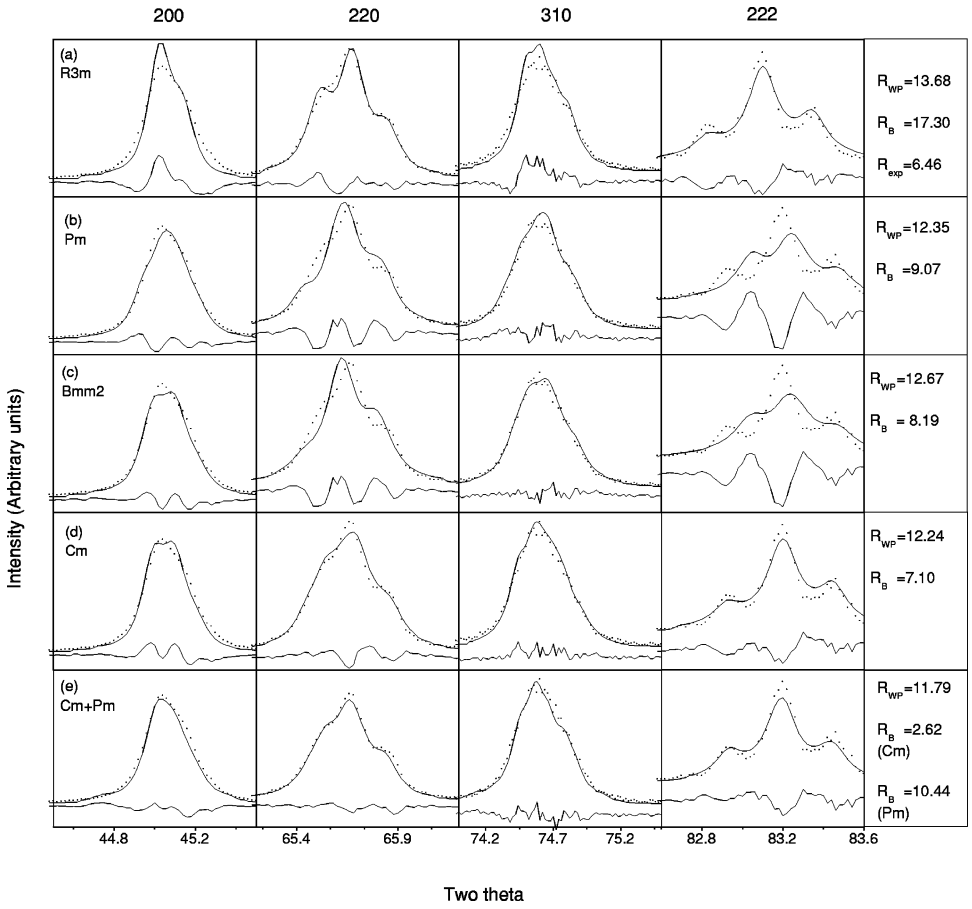

FIG. 4. Observed (dots), calculated (continuous line), and difference (bottom line) profiles of the 200, 220, 310, and 222 pseudocubic reflections obtained after the Rietveld refinement of PMN-xPT with $x=0.29$ using different structural models: (a) Rhombohedral R3m, (b) monoclinic Pm, (c) orthorhombic Bmm2, (d) monoclinic Cm, and (e) monoclinic Pm and Cm coexistence.

difference profiles alongwith the various agreement factors for the pseudocubic 200, 220, 310, and 222 reflections using four different space groups for $x=0.29$. For the R3mH space group [Fig. 4(a)], we see that the mismatch between the observed and calculated profiles is quite prominent for 200 and 310 pseudocubic reflections, which is also confirmed by highest value of the agreement factors. Thus R3mH space group is simply ruled out. For the space group Pm, the misfit between the observed and calculated profiles for the 220 and 222 pseudocubic reflections is very large. In particular, for the 222 pseudocubic profile, the observed and calculated peaks are appearing at different 2θ values ruling out the possibility of the Pm phase. A similar misfit for the 220 and 222 profiles is observed for the Bmm2 space group also as can be seen from Fig. 4(c). The Cm space group gives the most satisfactory fit between the observed and calculated profiles for all the four reflections as can be seen from Fig. 4(d). This is corroborated by the lowest value of the agreement factors also. Figure 5 depicts the observed, calculated, and difference profiles in the 2θ ranges 20–120 deg for $x=0.29$. The overall fit is quite satisfactory. The refined structural parameters are given in Table II. From an analysis of the refined positional coordinates given in Table II, it is found that the Cm phase of the PMN-xPT system is of M_B type ($Px=Py>Pz$) in contrast to the PZT system, where the Cm phase corresponds to the M_A type ($Px=Py<Pz$).[26]

C. Monoclinic structure with space group Pm ($0.31 \leqslant x \leqslant 0.34$)

On increasing the PT content beyond $x=0.30$, new features, like a shoulder in the 200 pseudocubic profile, appear. In order to determine the correct space group of PMN-xPT in

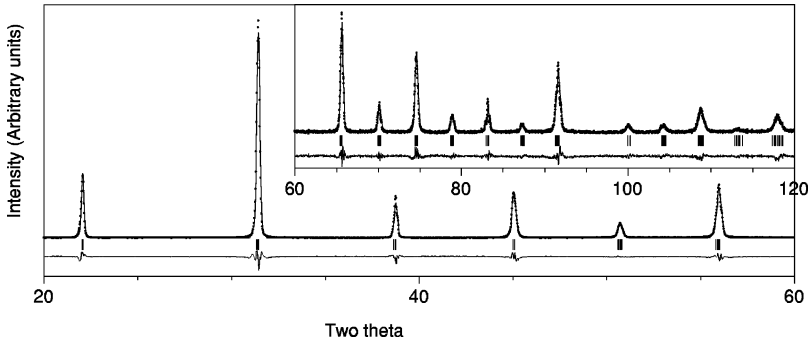

FIG. 5. Observed (dots), calculated (continuous line), and difference (bottom line) profiles obtained after the Rietveld refinement of PMN-xPT with $x=0.29$ using monoclinic space group Cm in the 2θ range 20–60 deg. Inset shows the patterns in the 2θ range 60–120 deg. Tick marks above the difference profle show peak positions for CuKα1.

TABLE II. Refined structural parameters of PMN-xPT for $x=0.29$ using monoclinic space group Cm.

Ions	Positional coordinates			Thermal parameters
	X	Y	Z	B (Å^2)
Pb^{2+}	0.00	0.00	0.00	3.08(2)
$Ti^{4+}/Nb^{5+}/Mg^{2+}$	0.5250(8)	0.00	0.498(2)	0.73(4)
O_I^{2-}	0.54(1)	0.00	−0.01(2)	0.2(3)
O_{II}^{2-}	0.317(2)	0.267(4)	0.48(1)	0.3(2)
$a=5.6951(2)$(Å)	$b=5.6813(2)$(Å)		$c=4.0138(1)$(Å)	$\beta=90.136(3)(°)$
$R_{WP}=12.24$	$R_{expt.}=6.46$		$R_B=7.10$	$\chi^2=3.59$

this composition range, we considered Cm, Bmm2, and Pm space groups in our Rietveld analysis. Figure 6. depicts the observed, calculated and difference profiles of PMN-xPT with $x=0.32$ for the pseudocubic 200, 220, and 310 reflections for the three space groups. It is evident from this figure that the best fit is obtained for the Pm space group which corresponds to the M_C phase in the notation of Vanderbilt and Cohen.[26] The agreement factors given in the last column of Fig. 6 are the lowest for the Pm space group. Figure 7 depicts the observed, calculated, and difference profiles in the 2θ range of 20–120 deg. The overall fit is quite satisfactory. Table III lists the refined structural parameters. It may be noted that the convention used for $\beta(>90)$ in Table II is different from that (<90)used in Ref. 16 as a result of which the positional coordinates also appear to be different.

D. Tetragonal structure with space group P4mm ($0.35\leqslant x\leqslant 1$)

The Rietveld analysis for $x\geqslant 0.35$ confirmed that the dominant phase of PMN-xPT for these compositions has got tetragonal structure. Very good fit between the observed and calculated profiles were obtained using tetragonal P4mm space group as can be seen from Fig. 8 for $x=0.39$. The refined structural parameters are listed in Table IV along with the agreement factors for this composition.

E. Phase coexistence

One often observes coexistence of neighboring phases in the MPB region due to extrinsic factors such as compositional fluctuations[39] and intrinsic factors such as a first-order phase transition between the low- and high-temperature phases.[12,13,15,40] The results of the preceding section show that in the PMN-xPT system, there are three phase boundaries occurring around $0.26<x<0.27$, $0.30<x<0.31$, and $0.34<x<0.35$ separating the stability fields of rhombohedral and Cm, Cm and Pm, and Pm and tetragonal phases, respectively. In order to see if further improvements in the agreement factors can result from a consideration of the coexistence of a minority neighboring phase, we carried out the Rietveld refinements for the composition ranges $0.27\leqslant x\leqslant 0.30$, $0.31\leqslant x\leqslant 0.34$, and $0.35\leqslant x\leqslant 0.39$ using various plausible coexisting phases. It was found that in the composition range $0.27\leqslant x\leqslant 0.30$, consideration of a minority

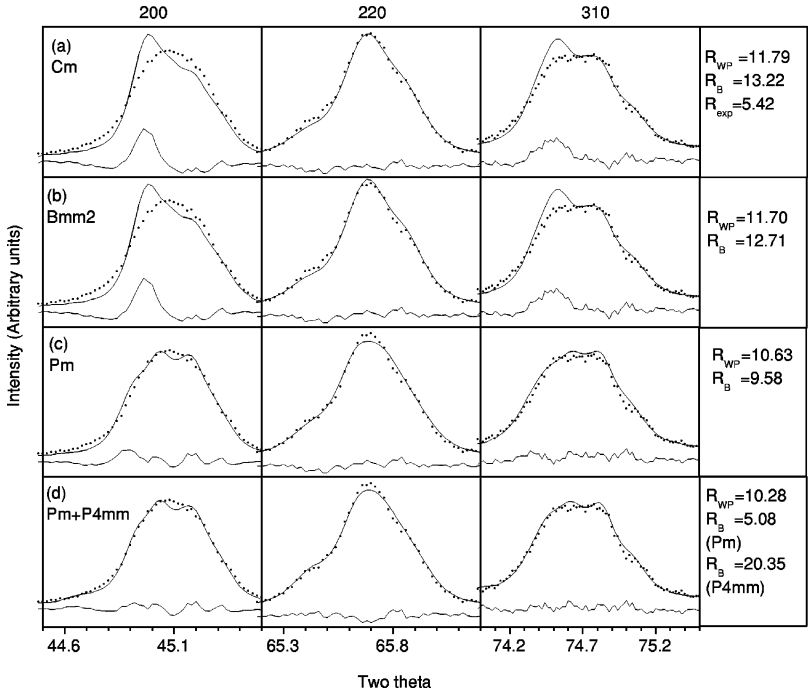

FIG. 6. Observed (dots), calculated (continuous line) and difference (bottom line) profiles of the 200, 220, and 310 pseudocubic reflections obtained after the Rietveld refinement of PMN-xPT with $x=0.32$ using different structural models: (a) Monoclinic Cm, (b) orthorhombic Bmm2, (c) monoclinic Pm, and (e) monoclinic Pm and tetragonal P4mm coexistence.

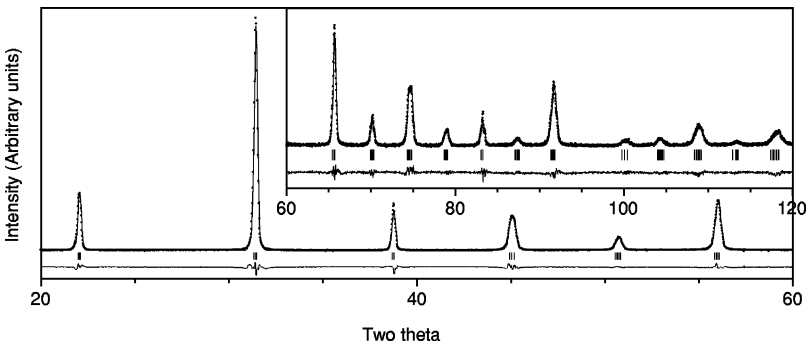

FIG. 7. Observed (dots), calculated (continuous line), and difference (bottom line) profiles obtained after the Rietveld refinement of PMN-xPT for $x=0.32$ using monoclinic space group Pm in the 2θ range 20–60 deg. Inset shows the patterns in the 2θ range of 60–120 deg. Tick marks above the difference profle show peak positions for CuKα1.

rhombohedral phase led to higher agreement factors, while minority monoclinic Pm phase decreased the agreement factors. The fits between observed and calculated profiles have improved for the (Cm+Pm) model as can be seen from a comparison of Fig. 4(e) with Fig. 4(d). Similarly, for the composition range $0.31 \leqslant x \leqslant 0.34$, consideration of a minority tetragonal phase decreased the agreement factors, whereas the minority Cm phase increased the agreement factors. The presence of minority tetragonal phase improves the fit, especially on the lower 2θ side of the 200 pseudocubic profile, as can be seen from a comparison of Fig. 6(c) with 6(d). Further, monoclinic Pm phase was found to coexist as a minority phase in the tetragonal region $0.35 \leqslant x \leqslant 0.39$ in agreement with the results of Ref. 23. The molar fractions of the minority and majority phases obtained by the Rietveld refinement are plotted in Fig. 9 as a function of PT content (x). It is evident from this figure that pure R3m phase exists for $x<0.27$. For $x=0.27$, the structure corresponds to that of pure Cm phase. On increasing the PT content (x), the Cm phase fraction decreases while the fraction of minority Pm phase increases. However, on crossing the Cm-Pm phase boundary at $0.30<x<0.31$, the fraction of the Pm phase increases abruptly. For $x=0.31$, the structure corresponds to pure Pm phase. On increasing x further (>0.31), the fraction of the majority Pm phase decreases, while that of the minority P4mm phase increases with increasing x in the composition range $0.31<x<0.35$. For compositions with $x>0.34$, the P4mm phase becomes the majority phase whose fraction increases with x, while the fraction of the minority Pm phase continuously decreases.

F. Variation of lattice parameters with composition

Variation of lattice parameters with composition (x) for the majority phase is plotted in Fig. 10 for $0.20 \leqslant x \leqslant 0.45$. The [100] and [010] directions of the tetragonal phase correspond to the [010] and [100] directions of the Pm phase, respectively. The [001] direction of the Pm phase deviates slightly from [001] direction of the tetragonal phase towards the [100] direction of the Pm phase giving rise to a monoclinic cell with unique b axis. The [100] and [010] directions of the Cm phase, on the otherhand, are along the $\langle 110 \rangle$ directions of the Pm and tetragonal phases. The cell parameters a_m, b_m of the Cm phase are related to the elementary perovskite cell parameters a_p, b_p as $a_p \approx a_m/\sqrt{2}$ and $b_p \approx b_m/\sqrt{2}$. For the sake of easy comparison with the corresponding cell parameters of the tetragonal and Pm phases, we have plotted a_p and b_p instead of a_m, b_m for the Cm phase in Fig. 10. In order to maintain the polarization rotation path[9,26] in going from tetragonal to Pm to Cm phases, for which $Pz \neq 0$ (Px, $Py=0$), $Pz \neq Px \neq 0$ ($Py=0$), and $Px=Py \neq 0$, $Pz \neq 0$, respectively, the a, b, c axes of the Pm phase become b_p, c_m, a_p, respectively, of the Cm phase. It is evident from Fig. 10 that for the tetragonal compositions, the a parameter increases while the c parameter decreases continuously with decreasing x. Around $0.34<x<0.35$, the a parameter of the tetragonal phase matches with the b parameter of the monoclinic (Pm) phase while the c parameter of the tetragonal phase, which remains as the c parameter of the Pm phase, shows a discontinuous drop. The a and c parameters of the Pm phase are nearly independent of composition, but the b parameter increases continuously with decreasing x. Further, the monoclinic angle β decreases continuously with decreasing x in the Pm phase field. The b, a, and c parameters of the Pm phase, which become c_m, b_p, and a_p of the Cm phase, do not show any discontinuity at the Pm-Cm phase boundary. Similarly, there is no discontinuous change

TABLE III. Refined structural parameters of PMN-xPT for $x=0.32$ using monoclinic space group Pm.

Ions	Positional coordinates			Thermal parameters
	X	Y	Z	B(Å^2)
Pb^{2+}	0.00	0.00	0.00	3.28
$Ti^{4+}/Nb^{5+}/Mg^{2+}$	0.509(2)	0.50	0.5479(7)	0.20(3)
O_I^{2-}	0.47(1)	0.00	0.57(1)	0.2(2)
O_{II}^{2-}	0.417(8)	0.50	0.059(6)	0.2(2)
O_{III}^{2-}	−0.02(1)	0.50	0.57(1)	0.0(3)
$a=4.0183(2)$(Å)	$b=4.0046(1)$(Å)		$c=4.0276(2)$(Å)	$\beta=90.146(3)(^\circ)$
$R_{WP}=10.63$	$R_{expt.}=5.42$		$R_B=9.56$	$\chi^2=3.84$

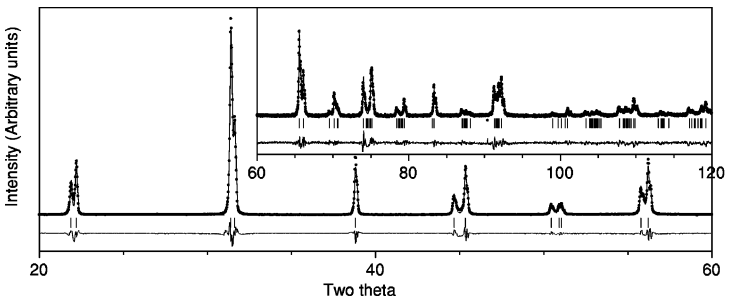

FIG. 8. Observed (dots), calculated (continuous line), and difference (bottom line) profiles obtained after the Rietveld refinement of PMN-xPT with $x=0.39$ using tetragonal space group P4mm in the 2θ range 20–60 deg. Inset shows the patterns in the 2θ range 60–120 deg. Tick marks above the difference profle show peak positions for CuKα1.

in the b_p and c_m cell parameters at the Cm-R3m phase boundary but a_p drops discontinuously. Table V lists the lattice parameter values of the majority phases for all the compositions studied by us.

G. Comparison of our results with earlier work

Singh and Pandey[16] first reported the stability of M_C phase with Pm space group at room temperature in the MPB region of PMN-xPT for $x=0.34$. In an independent study, Kiat *et al.*[17] reported M_C phase for $x=0.35$ at 90 K. Subsequently, Noheda *et al.*[23] confirmed that the M_C phase is the majority phase of PMN-xPT in the composition range $0.30<x<0.35$, which is consistent with the present findings also (see Fig. 9). Noheda *et al.*[23] have analyzed the XRD profiles of samples with $x=0.30$ and 0.39, which according to them possess rhombohedral and tetragonal structures, respectively. The main finding is that the so-called rhombohedral composition $x=0.30$ exhibits very pronounced anisotropic peak broadening which is absent in the tetragonal composition $x=0.39$. In particular, it is found that for $x=0.30$, the h00 reflections are maximum broadened, followed by hh0 reflections and then the hhh reflections. It is generally believed in the literature[5,17] that Pb^{2+} based compounds exhibit anisotropic peak broadening. However, the fact that only the composition $x=0.30$, and not $x=0.39$, for the PMN-xPT system exhibits anisotropic peak broadening suggests that the origin of such peak broadening is structure sensitive and not a general feature for all the phases in this system.The Williamson-Hall plot for $x=0.39$ given in Ref. 23 clearly reveals that the peak broadening is isotropic and is essentially due to compositional fluctuations and small coherently scattering domain size, since both $\Delta d/d$ and the intercept on the y axis are nonzero. For the composition $x=0.30$, there are three different slopes giving three different values for $\Delta d/d$ but only one intercept on the y axis. It is hard to believe that compositional heterogeneities can lead to anisotropic peak broadening for one composition ($x=0.30$), but not for the other ($x=0.39$) in samples prepared by the same method under identical conditions. The possibility of anisotropic peak broadening being due to the highly anisotropic coherently scattering domain size is also ruled out, since all the three straight lines corresponding to h00, hh0, and hhh reflections in the Williamson-Hall plots for $x=0.30$ intersect the y axis at the same point (see Fig. 3 of Ref. 23).

In a recent work on PZN-0.08PT single crystals, Ohwada *et al.*[41] have shown that the so-called rhombohedral structure is not rhombohedral, but possesses a different symmetry with "c" parameter less than "a" similar to the M_B phase with Cm space group as shown in Fig. 10 of the present work. The analysis of Ohwada *et al.*[41] shows that the peak center of 002 is shifted to higher **q** compared with that of 200 which is irreconcilable with the rhombohedral symmetry. In the related PZT system, Ragini *et al.*[12] have reported that the anomalous broadening of h00 reflections of the so-called rhombohedral phase shows a very systematic variation with composition for $0.530\leqslant x\leqslant 0.60$. Similar to the case of PMN-xPT,[23] this anomalous broadening is structure sensitive and is absent in the tetragonal ($0\leqslant x\leqslant 0.520$) and monoclinic compositions of PZT.[12] This anomalous broadening is inconsistent with the R3m space group since the h00 reflection is a singlet. It can, however, be accounted for in terms of the Cm space group.[12] A similar anomalous broadening in the $Pb(Fe_{0.5}Nb_{0.5})O_3$ system has been attributed to the Cm space group.[38] Thus there is sufficient evidence to suggest that the hitherto believed rhombohedral compositions in the PZT, PZN-xPT, and $Pb(Fe_{0.5}Nb_{0.5})O_3$ do not possess rhombohedral symmetry.

In the PMN-xPT system, our dielectric data clearly reveals the existence of a new phase between the R3m and Pm

TABLE IV. Refined structural parameters of PMN-xPT for $x=0.39$ using tetragonal space group P4mm.

Ions	Positional coordinates			Thermal parameters
	X	Y	Z	$B(\text{Å}^2)$
Pb^{2+}	0.00	0.00	0.00	2.92(1)
$Ti^{4+}/Nb^{5+}/Mg^{2+}$	0.50	0.50	0.532(1)	0.76(4)
O_I^{2-}	0.50	0.50	0.054(4)	0.8(3)
O_{II}^{2-}	0.50	0.00	0.601(2)	0.4(2)
$a=3.9920(0)$(Å)	$c=4.0516(1)$(Å)			
$R_{WP}=13.85$	$R_{expt.}=6.75$		$R_B=10.12$	$\chi^2=4.21$

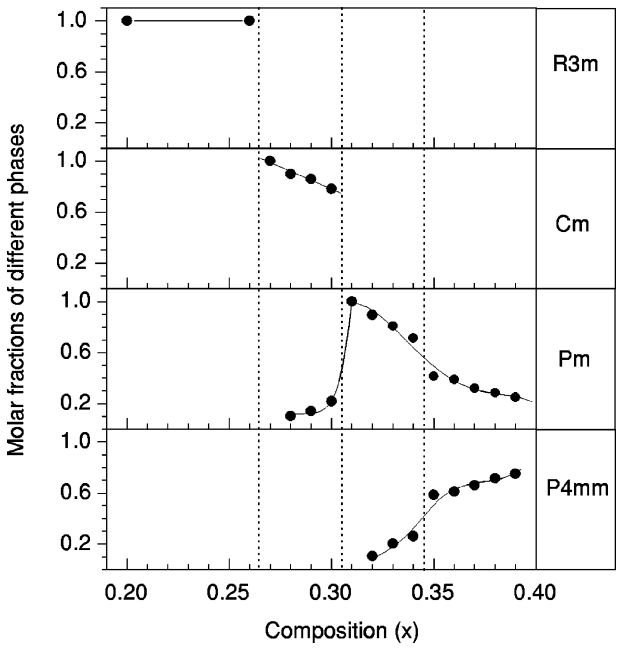

FIG. 9. Variation of molar fractions of different phases with composition (x) as obtained by the Rietveld refinement.

(M_C) compositions. According to Vanderbilt and Cohen's theory,[26] M_B phase (with Cm space group) should occur in between the rhombohedral and M_C (Pm space group) phase regions. Our Rietveld analysis of the XRD data indeed confirms the existence of M_B phase with space group Cm between the M_C and rhombohedral compositions.

In the PZT system, Corker *et al.*[14] have reported that acceptable R factors in the Rietveld analysis of neutron powder diffraction data for the so-called rhombohedral compositions could not be obtained unless local cationic displacements in the $\langle 110 \rangle$ directions are invoked. These local displacement directions in the light of the discovery of the monoclinic phase by Noheda *et al.*[4] correspond to the monoclinic [100] and [010] directions. It is obvious from the experimental facts presented in the preceding paragraphs as well as the findings of Corker *et al.*[14] that some of the compositions in these MPB systems, which were earlier regarded as rhombohedral, do not possess rhombohedral symmetry as a result of local monoclinic displacements. The Williamson-Hall plots for PMN-xPT system have revealed much smaller coherently scattering domain size of about 0.2 μm for such compositions as compared with that for the tetragonal composition for which it is 0.5 μm.[23] Since the monoclinic distortions are small and correlated monoclinic displacements occur over very small regions ($\sim$0.2 μm), the characteristic monoclinic splittings are not observable in the XRD pattern due to the large broadening of the individual profiles for small coherently scattering domain size. As a result, the only signature of a lower symmetry phase in such compositions is found in the anomalous anisotropic peak broadening, as was first reported by Ragini *et al.*[12] in the PZT context, and now observed in the present work also. Both in PZT (Ref. 12) and PMN-xPT, anomalous anisotropic peak broadening can be accounted for if one uses Cm space group in the Rietveld refinement. In the absence of any observable monoclinic splitting, the observed powder diffraction pattern from such compositions mimicks that expected for the rhombohedral phase, except, of course, for the anomalous anisotropic peak broadening of some reflections. In view of such a similarity of the powder diffraction patterns, some workers prefer to use the term ''average rhombohedral structure with local monoclinic displacements'' for such compositions. Such usage may be accepted only if one knows very clearly that the true structure is definitely not rhombohedral but monoclinic as a result of local $\langle 110 \rangle$ displacements.

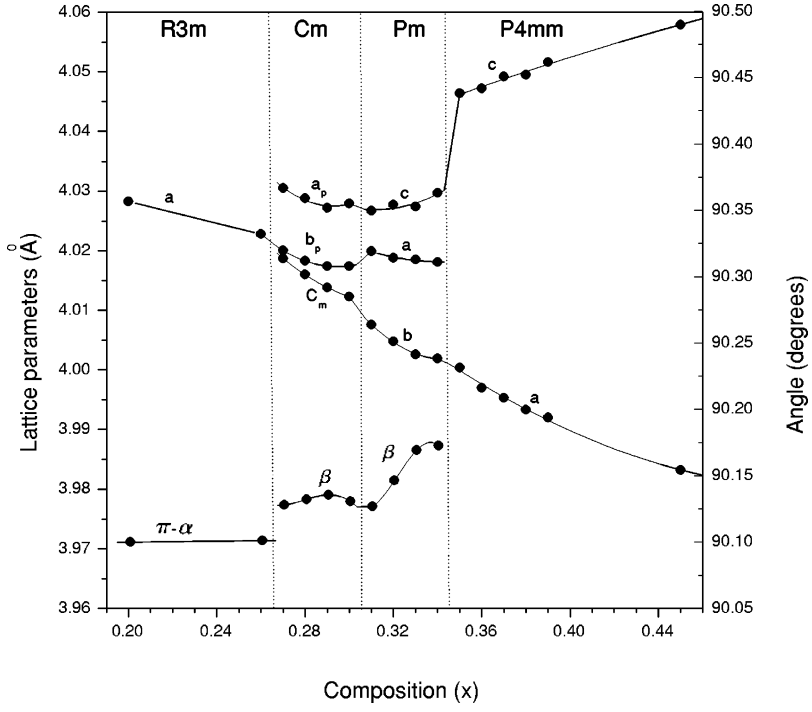

FIG. 10. Variation of lattice parameters with composition (x) for the majority phases of PMN-xPT.

TABLE V. Refined cell parameters of PMN-xPT for the majority phases in the composition range $0.20 \leqslant x \leqslant 0.45$.

Composition (x)	Cell parameters a(Å)	b(Å)	c(Å)	β(degree)
0.20	5.6921(1)		6.9882(2)	
0.26	5.6841(1)		6.9800(1)	
0.27	5.7001(2)	5.6852(2)	4.0186(1)	90.126(3)
0.28	5.6975(2)	5.6814(2)	4.0159(2)	90.133(3)
0.29	5.6953(2)	5.6813(2)	4.0138(1)	90.136(3)
0.30	5.6962(3)	5.6806(2)	4.0123(2)	90.131(3)
0.31	4.0193(2)	4.0082(2)	4.0288(2)	90.145(3)
0.32	4.0183(2)	4.0046(1)	4.0276(2)	90.146(3)
0.33	4.0185(2)	4.0026(1)	4.0274(1)	90.169(2)
0.34	4.0174(2)	4.0019(2)	4.0289(2)	90.177(3)
0.35	4.0004(1)		4.0464(1)	
0.36	3.9970(1)		4.0468(1)	
0.37	3.9953(1)		4.0492(1)	
0.38	3.9933(0)		4.0495(1)	
0.39	3.9920(0)		4.0516(1)	
0.45	3.9832(1)		4.0579(1)	

Before we close this discussion, we would like to mention that we also considered the possibility if the anisotropic peak broadening for $0.27 \leqslant x \leqslant 0.30$ compositions can be due to the compositional fluctuations and not due to the presence of a lower symmetry phase. For this, we carried out the Rietveld refinement for the composition $x=0.29$ using GSAS program package[31] which incorporates anisotropic peak shape proposed by Stephens.[32] Figure 11 shows the observed, calculated, and difference profiles for the (i) pseudocubic 200, 220, 310, and 222 reflections using R3m space group with isotropic and anisotropic peak profiles and (ii) Cm space group with isotropic peak profiles. As can be seen from Figs. 11 (a) and (b), the use of the anisotropic peak profiles somewhat improves the fit for 200 and 310 pseudocubic reflections, but fails to give satisfactory fit for 220 and 222 pseudocubic reflections. In fact, use of anisotropic peak profile leads to more mismatch between observed and calculated patterns near the 220 and $22\overline{2}$ reflections of the rhombohedral phase. As can be seen from Fig. 11(c), Cm space group model with isotropic peak profiles gives better match for these two reflections. We also considered the effect of anisotropic peak profiles for the structure refinement using Cm space group, and found that it worsens the fitting near the 220 position of the ''rhombohedral'' structure. Thus it can be concluded that the observed broadening of the (h00) and (hh0) pseudocubic reflections for compositions with $0.27 \leqslant x \leqslant 0.30$ may be predominantly due to the presence of a lower symmetry phase having space group Cm.

VI. CONCLUDING REMARKS

The phase diagram of Vanderbilt and Cohen[26] for an eighth-order expansion of the free energy predicts the stability regions of three types of monoclinic phases, M_A, M_B, M_C, in addition to the tetragonal (T), rhombohedral (R), and orthorhombic (O) phases (see Fig. 12). The R-M_A-T sequence of phase transition observed in PZT as a function of composition has been attributed to the region near $\alpha = \pi/2$, $\beta = 0.102$ by Vanderbilt and Cohen. For the PMN-xPT system, we have shown that the stable phases in the composition ranges $x<0.27$, $0.26<x<0.31$, $0.30<x<0.35$, and $x>0.34$ correspond to R, M_B, M_C, and T phases, respectively. In the phase diagram shown in Fig. 12, the R-phase region is followed by a narrow stability region of the M_B phase in broad agreement with our observations. However, as per this phase diagram, the M_B and M_C regions should be separated by a very thin orthorhombic (O) phase region. According to our Rietveld analysis results, the $M_B - M_C$ phase boundary occurs around $0.30<x<0.31$. Interestingly, in the Rietveld refinement for $x=0.30$, which is near this phase boundary, we found that M_B, M_C, and O

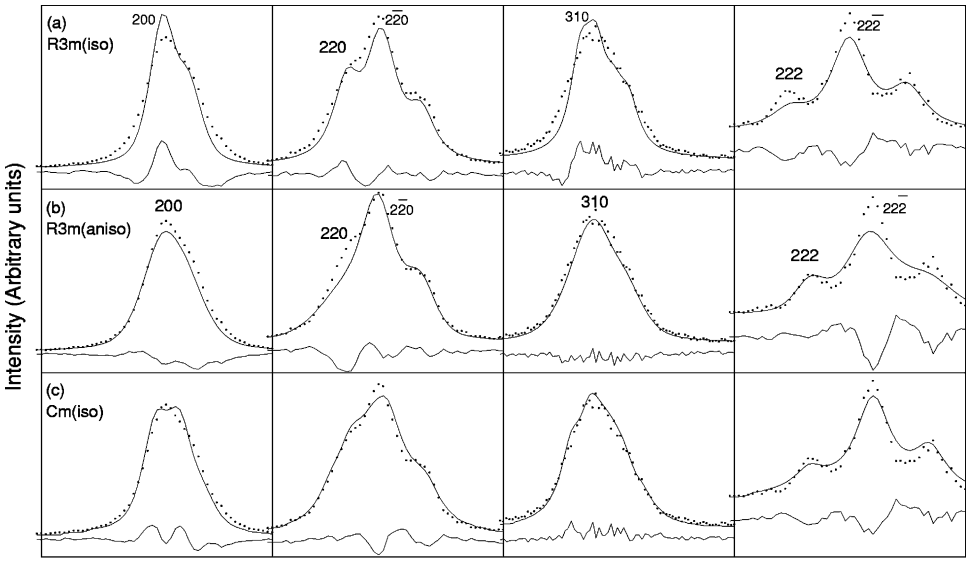

FIG. 11. Observed (dots), calculated (continuous line), and difference (bottom line) profiles of the 200, 220, 310, and 222 pseudocubic reflections obtained after the Rietveld refinement of PMN-xPT with $x=0.29$ using (a) rhombohedral R3m structure with isotropic peak profile, (b) rhombohedral R3m structure with anisotropic peak profile, (c) monoclinic Cm structure with isotropic peak profile.

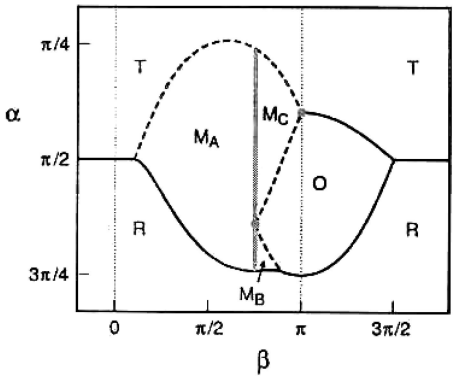

FIG. 12. Phase diagram for ferroelectric perovskites in the space of the dimensionless parameters α (vertical axis) and β (horizontal axis) (after Ref. 26).

phases give the same value of R_{WP} (12.92), but the R_B is the lowest for the O phase ($R_B = 12.84$, 10.04, 9.92 for the M_B, M_C and O phases, respectively) raising the possibility of the existence of the O phase in between the M_B and M_C phase regions. Thus the phase transition sequence R-M_B-O-M_C-T predicted by Vanderbilt and Cohen for $3\pi/4 < \beta < 0.8\pi$ may indeed correspond to the PMN-xPT system. Obviously, the structure of the PMN-xPT system in the MPB region is much more complex as compared to that in the PZT system with a simple R-M_A-T sequence of phase transitions. The polarization rotation path corresponding to the succession of phase transitions from rhombohedral to M_B to O to M_C to tetragonal in the PMN-xPT system is shown in Fig. 13. Although Vanderbilt and Cohen's theory predicts that R-M_B phase boundary to be of first-order type, our Rietveld analysis does not reveal any coexistence of R and M_B phases. However, since the nature of the XRD profiles for the two phases are quite similar, except for the anomalous broadening of h00 and hh0 reflections for the M_B phase, it may never be possible to settle the issue of coexistence of these two phases in a reliable fashion by the Rietveld refinement. The coexistence of M_C and T phases revealed by our Rietveld analysis is not expected on the basis of the Vanderbilt and Cohen's theory, since the corresponding boundary is of second-order type. This could be due to the limitations of the eighth-order truncation of the free-energy expansion.[42]

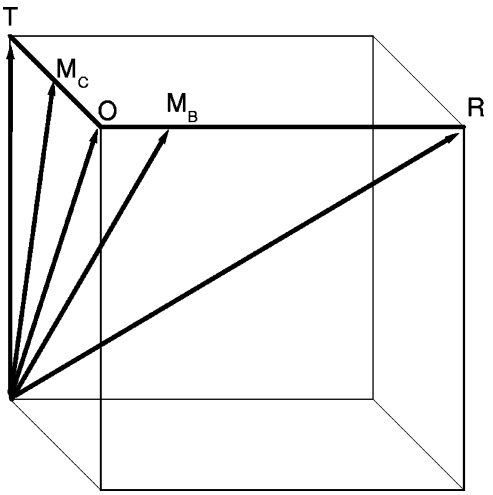

FIG. 13. Polarization rotation path for the crystallographic phases of the PMN-xPT system as per the theory of Vanderbilt and Cohen (after Ref. 26)

In the PZN-xPT system, there is some controversy about the structure of the MPB phase. According to Orauttapong *et al.*,[21] the sequence of phase transition in unpoled samples is R-O-T which is expected for $\pi < \beta < 3\pi/2$ in the Vanderbilt and Cohen's phase diagram. Kiat *et al.* have,[17] however, shown that the structure of PZN-xPT in the MPB region for $x = 0.09$ corresponds to the M_C phase. If it is so, we suspect the existence of M_B phase and possibly O phase also interposed between R and M_C phases, similar to what we have observed in the present study on the PMN-xPT system. The so-called "X" phase reported by Ohwada *et al.*[41] may indeed corespond to the M_B phase. It is likely that the relaxor ferroelectric based MPB systems may have similar sequence of phase transitions. Further, we suspect that the higher electromechanical response of these relaxor based MPB systems may be linked with the ease of polarization rotation in the presence of M_B, M_C, and probably O phases in the morphotropic phase boundary region as compared to the presence of only one phase (M_A) in the PZT system.

ACKNOWLEDGMENT

A.K.S. thanks UGC-BHU for financial support.

*Email address: dpandey@banaras.ernet.in

[1] S.-E. Park and T.R. Shrout, J. Appl. Phys. **82**, 1804 (1997).
[2] D. Viehland, A. Amin, and J.F. Li, Appl. Phys. Lett. **79**, 1006 (2001).
[3] B. Jaffe, W. R. Cook, and H. Jaffe, Piezoelectric Ceramics (Academic Press, London, 1971).
[4] B. Noheda, J.A. Gonzalo, L.E. Cross, R. Guo, S.-E. Park, D.E. Cox, and G. Shirane, Phys. Rev. B **61**, 8687 (2000).
[5] B. Noheda, D.E. Cox, G. Shirane, R. Guo, B. Jones, and L.E. Cross, Phys. Rev. B **63**, 014103 (2000).
[6] Ragini, S.K. Mishra, D. Pandey, H. Lemmens, and G. VanTendeloo, Phys. Rev. B **64**, 054101 (2001).
[7] R. Ranjan, Ragini, S.K. Mishra, D. Pandey, and B.J. Kennedy, Phys. Rev. B **65**, 060102(R) (2001).
[8] D.M. Hatch, H.T. Stokes, R. Ranjan, Ragini, S.K. Mishra, D. Pandey, and B.J. Kennedy, Phys. Rev. B **65**, 212101 (2002).
[9] H. Fu and R.E. Cohen, Nature (London) **403**, 281 (2000).
[10] L. Bellaiche and D. Vanderbilt, Phys. Rev. Lett. **83**, 1347 (1999); L. Bellaiche, A. Garcia, and D. Vanderbilt, *ibid.* **84**, 5427 (2000).
[11] R. Guo, L.E. Cross, S.-E. Park, B. Noheda, D.E. Cox, and G. Shirane, Phys. Rev. Lett. **84**, 5423 (2000).
[12] Ragini, R. Ranjan, S.K. Mishra, and D. Pandey, J. Appl. Phys. **92**, 3266 (2002).
[13] S.K. Mishra, A.P. Singh, and D. Pandey, Philos. Mag. B **76**, 213 (1997); **76**, 227 (1997).
[14] D.L. Corker, A.M. Glazer, R.W. Whatmore, A. Stallard, and F. Fauth, J. Phys.: Condens. Matter **10**, 6251 (1998).
[15] D. Pandey and Ragini, Z. Kristallogr. **218**, 1 (2003).

[16] A.K. Singh and D. Pandey, J. Phys.: Condens. Matter **13**, L931 (2001).
[17] J.M. Kiat, Y. Uesu, B. Dkhil, M. Matsuda, C. Malibert, and G. Calvarin, Phys. Rev. B **65**, 064106 (2002).
[18] Y. Lu, D.-Y. Jeong, Z.-Y. Cheng, Q.M. Zang, H.-S. Luo, Z.-W. Yin, and D. Viehland, Appl. Phys. Lett. **78**, 3109 (2001).
[19] Z.-G. Ye, B. Noheda, M. Dong, D. Cox, and G. Shirane, Phys. Rev. B **64**, 184114 (2001).
[20] G. Xu, H. Luo, H. Xu, and Z. Yin, Phys. Rev. B **64**, 020102 (2001).
[21] D. La-Orauttapong, B. Noheda, Z.-G. Ye, P.M. Gehring, J. Toulouse, D.E. Cox, and G. Shirane, Phys. Rev. B **65**, 144101 (2002).
[22] M.K. Derbin, J.C. Hicks, S.-E. Park, and T.R. Shrout, J. Appl. Phys. **87**, 8159 (2000).
[23] B. Noheda, D.E. Cox, G. Shirane, J. Gao, and Z.-G. Ye, Phys. Rev. B **66**, 054104 (2002).
[24] B. Noheda, D.E. Cox, G. Shirane, S.-E. Park, L.E. Cross, and Z. Zhong, Phys. Rev. Lett. **86**, 3891 (2001).
[25] K. Ohwada, K. Hirota, P. Rehrig, P.M. Gehring, B. Noheda, Y. Fujii, S.-E. Park, and G. Shirane, J. Phys. Soc. Jpn. **70**, 2778 (2001).
[26] D. Vanderbilt and M.H. Cohen, Phys. Rev. B **63**, 094108 (2001).
[27] A. K. Singh and D. Pandey (unpublished).
[28] S.L. Swartz and T.R. Shrout, Mater. Res. Bull. **17**, 1245 (1982).
[29] O. Bouquin and L. Martine, J. Am. Ceram. Soc. **74**, 1152 (1991); H.C. Wang and W.A. Schulze, *ibid.* **73**, 825 (1990).
[30] R. A. Young, A. Sakthivel, T. S. Moss, and C. O. Paiva Santos, Program DBWS-9411 for Rietveld Analysis of x ray and Neutron Powder Diffraction Pattern, 1994.
[31] A. C. Larson and R. B. Von Dreele, computer code GSAS. (Los Alamos National Laboratory, Los Alamos, 2000).
[32] P.W. Stephens, J. Appl. Crystallogr. **32**, 281 (1999).
[33] A.M. Glazer and S.A. Mabud, Acta Crystallogr., Sect. B: Struct. Crystallogr. Cryst. Chem. **B34**, 1065 (1978).
[34] H.D. Megaw and C.N.W. Darlington, Acta Crystallogr., Sect. A: Cryst. Phys., Diffr., Theor. Gen. Crystallogr. **A31**, 161 (1975).
[35] H. D. Megaw, *Ferroelectricity in Crystals* (Methuen & Co. Ltd., London, 1957).
[36] S.L. Swartz, T.R. Shrout, W.A. Schulze, and L.E. Cross, J. Am. Ceram. Soc. **67**, 311 (1984).
[37] J. Kelly, M. Leonard, C. Tantigate, and A. Safari, J. Am. Ceram. Soc. **80**, 957 (1997).
[38] N. Lampis, P. Sciau, and A.G. Lehmann, J. Phys.: Condens. Matter **11**, 3489 (1999).
[39] K. Kakegawa, J. Mohri, K. Takahasi, H. Yamamura, and S. Shirasaki, Solid State Commun. **24**, 769 (1977).
[40] S.K. Mishra, A.P. Singh, and D. Pandey, Appl. Phys. Lett. **69**, 1707 (1996).
[41] K. Ohwada, K. Hirota, P.W. Rehrig, Y. Fujii, and G. Shirane, cond-mat/0207726 (unpublished).
[42] I.A. Sergienko, Y.M. Gufan, and S. Urazhdin, Phys. Rev. B **65**, 144104 (2002).